AIAA JOURNAL
Vol. 32, No. 6, June 1994

Coherent Structure in a Combusting Jet in Crossflow

Rong F. Huang* and Jean M. Chang†
National Taiwan Institute of Technology, Taipei, Taiwan 10672, Republic of China

The flame behavior and coherent structure of the combusting propane gas jet in a cross airstream at low jet-to-wind momentum flux ratios are studied experimentally. A one-component constant-temperature hot-wire anemometer is employed to extract frequency information from the traveling coherent structures evolving from the upwind side of the jet body. The reduced traveling frequency of the coherent structure in the near burner region is correlated to the jet-to-wind momentum flux ratio. The reduced eddy traveling frequency approaches to a constant of about 0.35 at high jet-to-wind momentum flux ratios. The trajectories of the traveling coherent structures depicted by the bisector of the eddy traveling avenue (the narrow band where the coherent structures sweep over) are correlated by nondimensional coordinates. The coherent structure is found to be profoundly related to the split and flickering phenomena of the flames in the jet momentum dominant region.

Nomenclature

d	= inner diameter of burner tube
E	= voltage output of hot-wire anemometer
f	= eddy traveling frequency (frequency of coherent structures passing through and detected by hot-wire probe)
J	= jet-to-wind momentum flux ratio, J_j/J_w
J_j	= momentum flux of fuel jet, $\rho_j u_j^2$
J_w	= momentum flux of crossflow, $\rho_w u_w^2$
R	= square root of jet-to-wind momentum flux ratio, $J^{1/2}$
St	= Strouhal number, fd/u_j
u_j	= average exit velocity of fuel jet
u_w	= average velocity of cross airflow
X, Y, Z	= Cartesian coordinates with origin at center of jet exit plane
$\bar{X}$	= nondimensional X coordinate of eddy traveling path, X/Rd
$\bar{Z}$	= nondimensional Z coordinate of eddy traveling path, Z/Rd
ρ_j	= mass density of fuel jet
ρ_w	= mass density of cross airflow
Φ	= spectral density function of E

Introduction

COHERENT structures have been noticed by investigators for their roles in the mixing rates in plane mixing layers[1] and in round jets.[2] A review of the uses of coherent structure was presented by Coles.[3] Considerable effort has been devoted to understanding the interaction of the organized structure and the flame characteristics in reacting plane shear layers[4–6] and axisymmetric gas jets.[7–10] The flame behavior, including liftoff, blowout, and hysteresis of vertical diffusion flames has been reported to be closely related to the dynamics of the shear-induced coherent structures.[11–14] The combusting gas jet in a crossflow can be placed into two categories. Figure 1 shows the sketches of the typical flames in burner-detached and *burner-attached* regimes. The flames in the *burner-detached* regime exist at high jet-to-wind momentum flux ratios. The combusting jet behaves like a crossflow-deflected diffusion flame.[15–22] The flames in the burner-attached regime exist at low jet-to-wind momentum flux ratios ($J <$ 20, in this study). The jet body is bent over severely so that the jet and burner tube serve as the flame holders which generate a flammable area in the recirculation region.[23] Two types of organized flow structures have been reported in the literature for the combusting jet in a crossflow. One is the pair of streamwise-oriented counter-rotating vortices, which exists at high jet-to-wind momentum flux ratios.[16] The other is the coherent structure on the upper bent jet surface in the near burner region, which was first presented in a schlieren picture by Huang et al.[23] for burner-attached flames. The counter-rotating vortices have been studied by many investigators due to their strong influence on jet or flame behavior. However, the roles of the coherent structure in a combusting jet in a crossflow have not been studied by investigators. In this paper, we present some results from a study of the burner-attached propane gas jet flames in a cross airflow in which the time-averaged flowfield is essentially symmetric about a vertical center plane. The results not only confirm the presence of coherent structures in the flow but also reveal the characteristic features and influence on the flame behavior. We focused our attention on the dynamics of the organized structure, the trajectory of the traveling coherent structures, and the influence of the large eddies on the flame behavior.

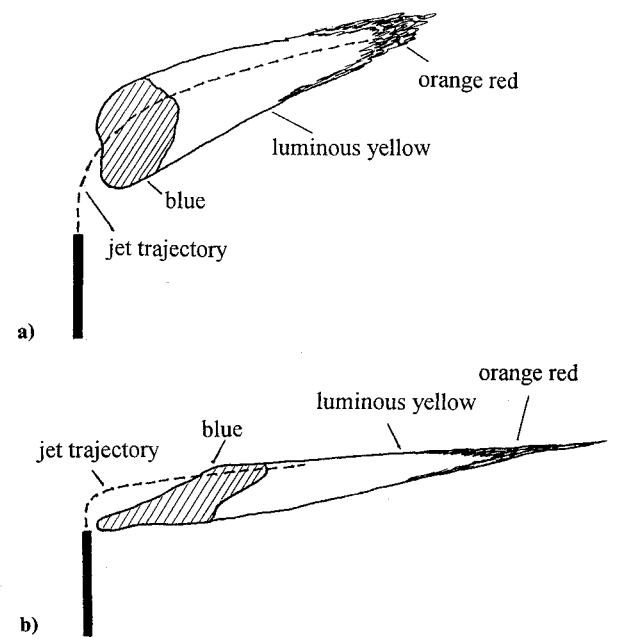

Fig. 1 Sketches of typical flames in crossflow in a) burner-detached regime and b) burner-attached regime.

Received Sept. 28, 1993; revision received Feb. 8, 1994; accepted for publication Feb. 10, 1994.

*Associate Professor, Department of Mechanical Engineering. Member AIAA.

†Research Assistant, Department of Mechanical Engineering.

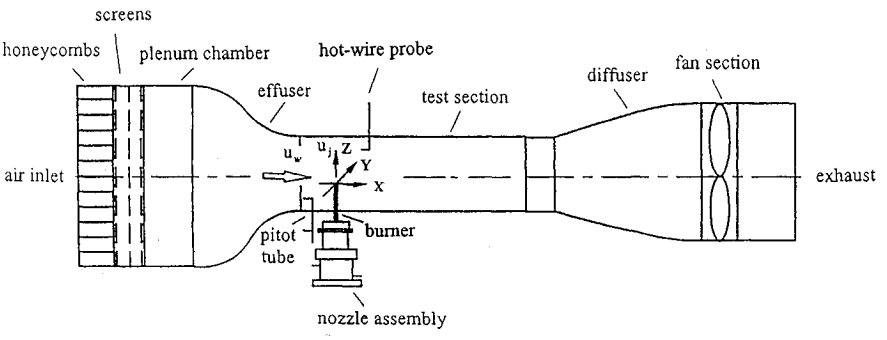

Fig. 2 Experimental setup and definition of coordinate system.

Experimental Details

Wind Tunnel and Combustor

The experiments are performed in a suction-type, open loop wind tunnel shown in Fig. 2. The wind tunnel has a test section of 30 × 30 × 110 cm. The test section is made with two polished aluminum alloy plates serving as the ceiling and the floor and two reinforced thermal-resistive plate glass panels serving as the side walls to allow for photography and visualization. The contraction ratio of the effuser is 9 to 1. Honeycombs and three layers of screens are placed at the inlet of the wind tunnel to reduce the turbulence intensity of the flow in the test section. The maximum turbulence intensity at a wind speed of 20 m/s measured by a hot-wire anemometer is less then 0.5%. During the experiments the velocity of the crossflow is monitored with a pitot-static tube.

The combustor is a stainless tube with an inner diameter of 5.0 mm, an outer diameter of 6.4 mm, and a length of 250 mm. The tube protrudes 180 mm into the wind tunnel through and perpendicular to the aluminum floor plate of the test section. Description is given in terms of a rectangular coordinate system (X, Y, Z), as shown in Fig. 2. The origin is centered at the exit plane of the burner tube. The burner tube is adapted to the tip of a nozzle assembly which serves as the flow conditioning and measuring device. The contraction ratio of the well-contoured nozzle is 324:1, which is large enough to ensure very slow motion in the settling chamber so that the total pressure can be accurately measured from the pressure tap on the wall of the settling chamber. The flow rate of the fuel jet is calculated using the dynamic pressure. The turbulence intensity of the issuing jet at the exit plane, except in the shear layer, is lower than 0.2% for an average exit velocity of 9.2 m/s at zero crosswind velocity. The fuel used in this study for combustion in the wind tunnel is commercial-grade propane with compositions of about 95.0% C_3H_8, 3.5% C_2H_6, and 1.5% C_4H_{10}.

Optical Photography

The short (down to 1/12,000 s) and long (about 2 s) time exposure direct color photography, shadowgraph, and schlieren optical techniques are employed to identify the flame modes and to distinguish the characteristics of the flow patterns. The shadowgraph and schlieren pictures are focused on the near burner region. A 1000 W xenon-mercury lamp is used as the light source and two 20-cm plane-convex lenses are employed to collimate the light path.

Experimental Procedure

The stability limits of the flame are outlined by slowly varying the flow rate of the fuel jet at a fixed crosswind velocity until the flame is blown out. At blowoff the crosswind and fuel jet velocities are recorded by a data acquisition system. The same procedure is repeated for various crosswind velocities from 4.5 to 18 m/s. The flame modes are identified by visual inspection and examination of the color flame pictures taken through the whole stability domain. The shadowgraph and schlieren techniques are then employed to mark the flow patterns. A one-component hot-wire probe operated at a constant temperature mode is placed on the center plane ($Y = 0$) at $X = 1.5$ cm and is adjusted to a Z position where the traveling eddies pass through. The most proper Z position of measurement is monitored from both the shadowgraph images on a screen and the output signals of the hot-wire anemometer on an oscilloscope. The hot-wire probe is made of a platinum wire which is 1.5 μm in diameter and 1.5 mm in length. The response capability of the anemometer is estimated to be at least 3000 Hz. The output signals of the hot-wire anemometer are fed to a PC-based data acquisition system to extract frequency information on the traveling eddies. The hot-wire probe is used here as a device to sense the frequency when the eddies pass through the wire, rather than as an accurate velocity measuring instrument. Only the passing-through frequency of the coherent structure is of concern here so the deviation caused by the effect of density variation is not corrected in this experiment.

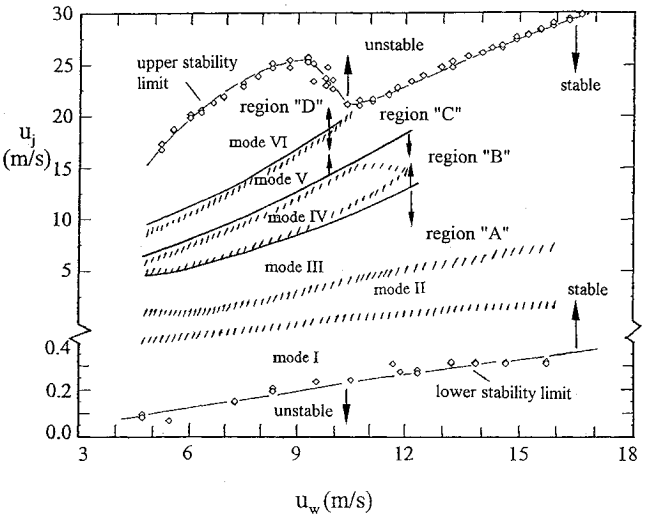

Fig. 3 Map for stability regimes, flame modes, and traveling coherent structure: mode I, down-washed flames; mode II, flashing flames; mode III, developing flames; mode IV, dual flames; mode V, flickering flames; mode VI, pre-blow-off flames; region A, cross-flow dominant; region B, transition; region C, fuel jet dominant; and region D, loss of coherency.

Results and Discussion

Flame Behavior

Figure 3 shows the stability domain of the propane gas jet flame in a crossflow obtained in this experimental study. There are two blowout limits associated with jet velocity. The area between the upper and lower limits in Fig. 3 represents the domain in which the flames are stabilized. The stability domain for burner-attached flames covers higher crossflow velocities and lower fuel jet velocities compared to the burner-detached flames.[15] Prior to blowoff, the flame base of the burner-attached flame always resides on the lee side of the bent jet body instead of lifting off the burner tip as in the case of the burner-detached flame.[16]

The flame configurations in the stability domain are identified by direct visual inspection and by short and long time exposure

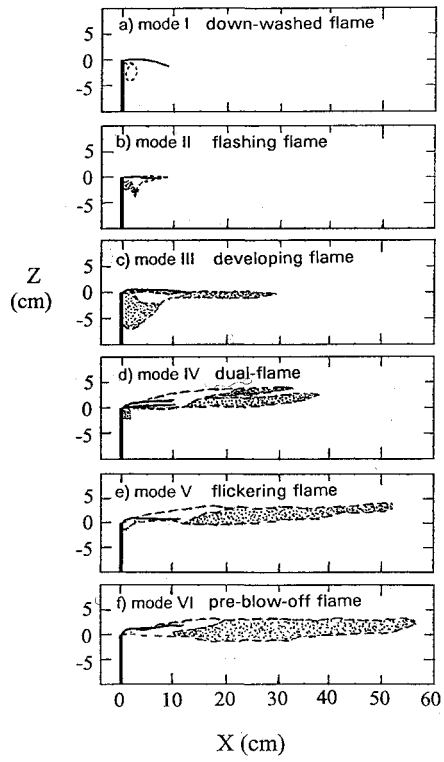

Fig. 4 Typical flame configurations at different characteristic modes: u_w = 4.86 m/s, u_j = a) 0.12 m/s, b) 1.40 m/s, c) 3.39 m/s, d) 5.53 m/s, e) 7.11 m/s, and f) 10.89 m/s; —— jet trajectory; ⌊ ⌋ blue zone; ▨ luminous orange zone.

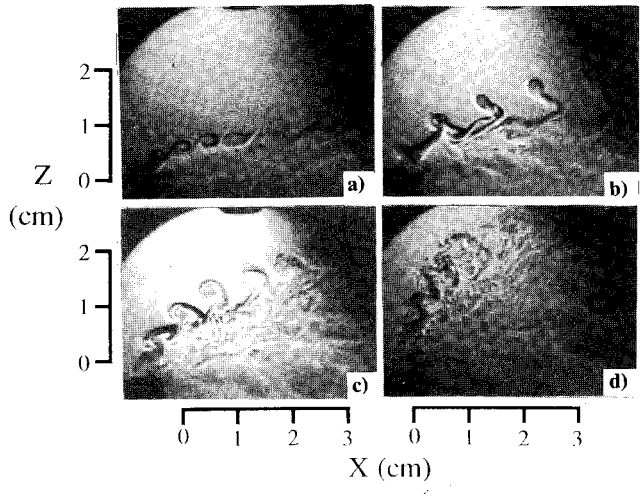

Fig. 5 Schlieren photographs of traveling coherent structures: u_w = 4.86 m/s, u_j = a) 3.64 m/s, region A; b) 6.15 m/s, region B; c) 8.50 m/s, region C; and d) 13.74 m/s, region D.

photography. Six typical characteristic modes are identified. The regions of the characteristic flame modes are marked by the short slashed lines in Fig. 3. Figure 4 shows the sketches of typical flames for each mode at u_w = 4.86 m/s. The dashed lines show the contours of the flames. The solid lines depict the bisector of the long time exposure shadowgraph images of the fuel jets. The blank areas enclosed by the slashed lines are blue flames and the dotted areas are luminous orange regions. In all cases, the jet trajectories in the near burner region are all located above the flames. The bent jet bodies are not enclosed by the flames until a few burner diameters downstream from the burner. The flame shown in Fig. 4a is in the region of mode I, in which flames are called down-washed flames. The jet-to-wind momentum flux ratio in mode I is very low and the flammable region is located around the recirculation area

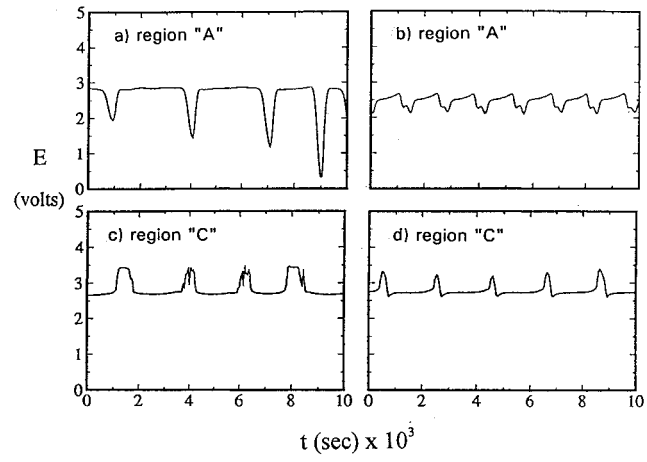

Fig. 6 Typical hot-wire signals at u_w = 4.86 m/s, region A: a) u_j = 2.47 m/s and b) u_j = 3.84 m/s. Region C: c) u_j = 6.88 m/s and d) u_j = 7.11 m/s. Data measured at sampling rate of 12,000 samples/s.

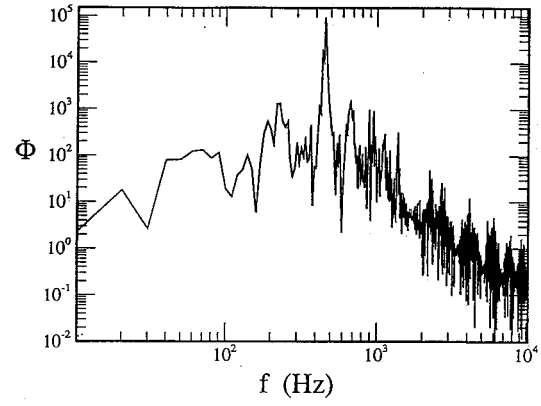

Fig. 7 Typical power spectral density function of hot-wire signals at u_w = 4.86 m/s and u_j = 5.34 m/s.

in the near wake of the tube. The jet body is flushed by the cross stream and curved downward to form a recirculation area due to the down-wash effect around the burner tip area. As the jet-to-wind momentum flux ratio is raised to the region of mode II, as is shown in Fig. 4b, the trajectory of the down-washed jet body in mode I is tilted up to align with the main stream and the intermittently flashing blue flame downstream of the down-washed flame is observed. Flames in mode II are called flashing flames. As the jet momentum is increased to the region of mode III, in which flames are called developing flames, the intermittency of the flashing blue flame finally stabilizes and stems itself from the down-washed flame area as is shown in Fig. 4c. The area of the blue and orange zones of the down-washed flame in mode II is enlarged as the momentum of the fuel jet is increased. The length of the flame in mode III elongates and the down-washed flame shrinks gradually as the jet momentum is increased. As the jet momentum increases to the region of mode IV, as is shown in Fig. 4d, the flames start shortening and the dual-flame patterns appear. The flame regains its elongation after it reaches the shortest length at which the dual-flame pattern is most obviously observed. In the region of mode V, as is shown in Fig. 4e, the flame becomes increasingly wider with an increase of jet momentum. In the down-washed area the soot-radiating orange zone disappears but the small blue flame in the recirculation area still exists. The soot-radiating zone in the downstream area grows and flickers, which causes the flames in this mode to be called flickering flames. This pattern remains the same until the jet momentum increases to the region of mode VI, as is shown in Fig. 4f. In mode VI the small blue flame in the recirculation area disappears and the flame length does not appreciably increase with jet velocity. Prior to blowoff,

the blue zone anchors at the lee side of the bent jet body above the tip of the burner instead of staying in the wake of the burner. No trace of flame in the recirculation area behind the burner is found.

Coherent Structure

The fuel jet issuing from the burner is subjected to the impingement and the shear of the crossflow. Although the interaction is three dimensional and complex, the average flowfield is symmetric about the center plane ($Y = 0$).[23] The coherent structure evolving from the upwind side of the jet body is observed in this experiment. The schlieren photographs in Fig. 5 show the different configurations of the coherent structures in the near burner region. As the flow conditions fall into region A of Fig. 3, the coherent structure has vorticity in the $+Y$ direction as is shown in Fig. 5a. In this region the momentum of the crossflow prevails over that of the fuel jet. The jet-to-wind momentum flux ratio is lower than about 0.9 in region A. Flame modes I, II, and III belong to region A. As the jet-to-wind momentum flux ratio increases to region B of Fig. 3, the direction of the vorticity of the coherent structure is hard to distinguish, as is shown in Fig. 5b. Mushroom-like flow structures are found in this region. The direction of the vorticity of the coherent structure is in transition from $+Y$ to $-Y$ for jet-to-wind momentum flux ratio increases from 0.9 to 1.2. The dual-flame mode belongs to this transition region. As the jet-to-wind momentum flux ratio increases to region C of Fig. 3, the coherent structure has vorticity in the $-Y$ direction, as is shown in Fig. 5c. In this region the momentum of the fuel jet prevails over that of the crossflow. The jet-to-wind momentum flux ratio in this region is higher than about 1.2. The flickering flame mode belongs to the region C. As the jet-to-wind momentum flux ratio increases to a level higher than about 3.5, as shown in region D of Fig. 3, the organized structure can no longer maintain distinguishable coherency, as is shown in Fig. 5d.

The typical signal output from the hot-wire anemometer, which is mounted in the wind tunnel to sense the motion of the traveling coherent structure, as shown in Fig. 6. The probe is placed on plane of $X = 1.5$ cm, where the jet body has been bent over to align with the main cross stream. Signals in Figs. 6a and 6b having characteristic peaks pointing downward indicate that the coherent structure is rolling in the $-Y$ direction (region A) when passing through the probe. Signals in Fig. 6b have a higher frequency than those in Fig. 6a. The jet momentum in Fig. 6b is higher than that in Fig. 6a. Signals in Fig. 6c and 6d having characteristic peaks pointing upward indicate that the coherent structure is rolling in the $+Y$ direction (region C) when passing through the probe. The signals in Fig. 6d have a slightly higher frequency than those in Fig. 6c. The jet momentum in Fig. 6d is a little higher than that in Fig. 6c. The signals switch patterns from peaks pointing downward to peaks pointing upward in the transition region B. Signals in region D which are not shown here show no apparent coherent peaks. The discrete Fourier transform is employed to convert the hot-wire raw data in the time domain to the power spectral density function in the frequency domain. Thus, the eddy traveling frequency is located at the peak of the power spectral density function. Figure 7

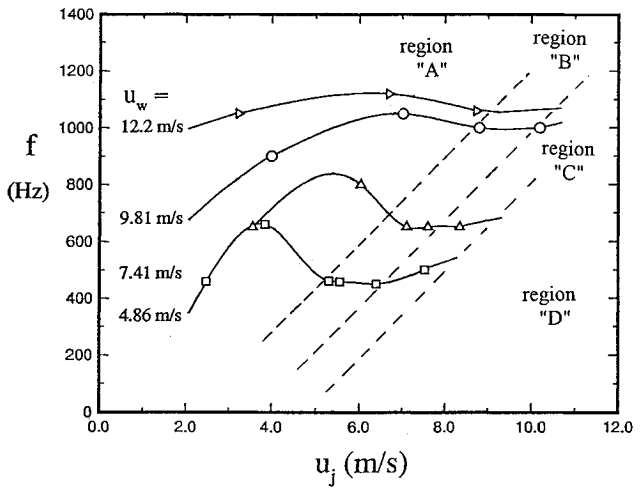

Fig. 8 Variation of traveling coherent structure frequency with jet velocity.

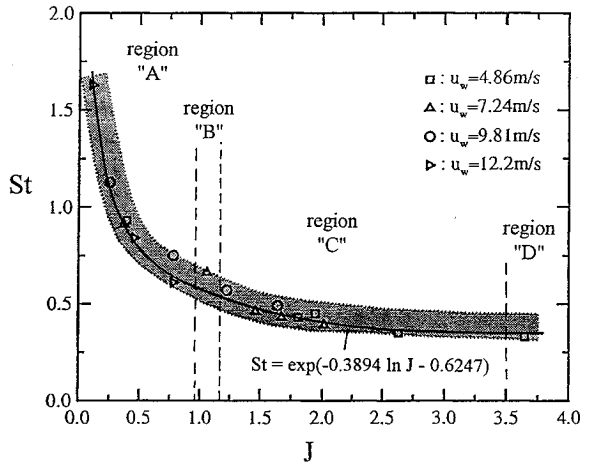

Fig. 9 Correlation of Strouhal number and jet-to-wind momentum flux ratio.

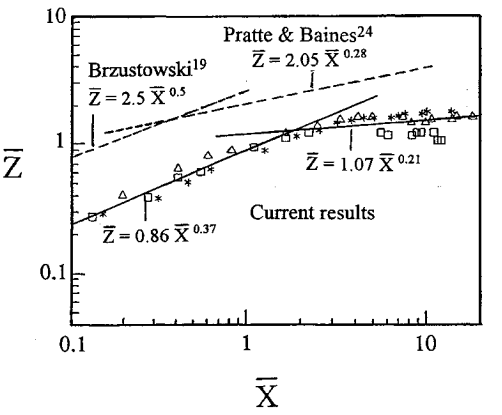

Fig. 10 Correlation of trajectory of traveling coherent structures.

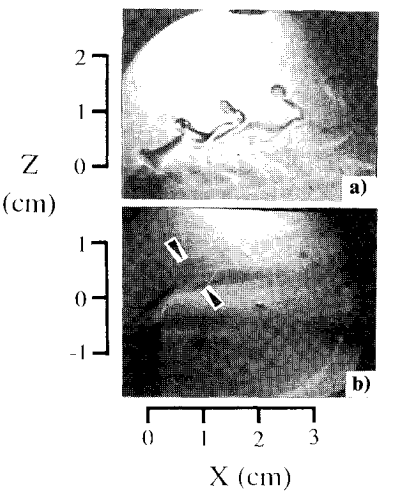

Fig. 11 Schlieren images of split fuel jet for dual flame at $u_w = 4.86$ m/s and $u_j = 6.15$ m/s: a) 1/12,000 s exposure and b) 1 s exposure; arrow heads in b) indicate the split streams.

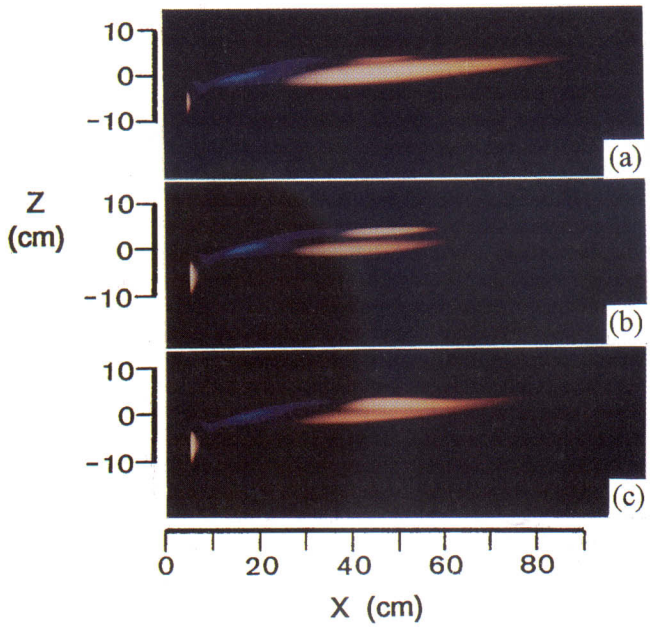

Fig. 12 Dual flames, u_w = 4.86 m/s and u_j = a) 5.39 m/s, b) 5.56 m/s, and c) 5.64 m/s.

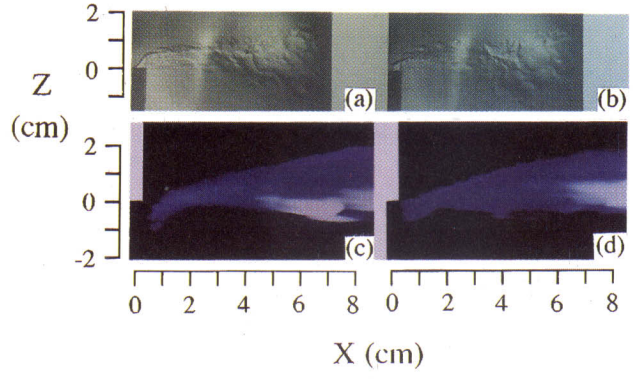

Fig. 13 Flickering flames at u_w = 4.86 m/s and u_j = 6.98 m/s, a) bright mode, b) bright mode, c) dark mode, and d) dark mode.

shows a typical power spectral density function in the frequency domain for u_w = 4.86 m/s and u_j = 5.34 m/s. The eddy traveling frequency is easily found in this plot to be 460 Hz. The variations of the eddy traveling frequency with jet velocity are shown in Fig. 8. For the four wind velocities shown in Fig. 8, the frequency varies much as it does similarly with jet velocity. The variations at low crossflow velocities are more prominent than they are at high crossflow velocities. In region A, the eddy traveling frequency increases with the fuel jet velocity to a peak value. After that it decreases with the jet velocity and reaches a minimum in transition region B. The frequency of the traveling eddies remains almost constant in region B. In region C, the traveling eddy frequency increases slowly with the fuel jet velocity. The behavior of the traveling coherent structure of the combusting jet in the crossflow is much more complicated than that in the freejet. The primary dominant factors are not only the effect of shear due to the jet/environment velocity difference, which was employed in the calculation of the celerity for the shear-layer by Coles,[3] but also the effect of the impingement by the crossflow on the jet body.

Although not verified here, we try to find a reason for the variations of the eddy traveling frequency by considering the shear and impingement effects. Consider the emanating jet around the near burner tip area. At very low jet-to-wind momentum flux ratios, the jet body is bent severely. The instability waves generated on the jet surface are primarily due to the shear effect caused by the wind. The undulated waves on the jet surface are stretched by shear in the bent jet direction, and hence have a long wavelength and a low frequency. As the jet-to-wind momentum flux ratio increases, but remains in region A, the jet body tilts upwards. The decrease of the stretching effect due to the decrease of shear in the bent jet direction causes the eddy wavelength to decrease. Hence the traveling frequency increases with jet velocity. As the bent jet body tilts higher than a critical angle with an increase of the jet velocity, the decrease of the shear effect on the jet surface prevails. This effect reduces the vortex generation rate, and hence, the eddy traveling frequency. As the jet-to-wind momentum flux ratio increases to the values in region B, the high tilt angle due to the high momentum of the fuel jet causes the effects of shear between the fuel jet and the cross stream boundary, and the impingement by the cross stream on the fuel jet to balance. The orientation of the vorticities of the coherent structures is in transition from $+Y$ to $-Y$ within a narrow margin of jet-to-wind momentum flux ratios. During this process the eddy traveling frequency does not vary appreciably with jet velocity. As the jet-to-wind momentum flux ratio increases to the value in region C, the high jet/wind velocity difference creates high shear on the jet surface in reverse direction to that in region A. The traveling frequency of the coherent structures thus increases with jet velocity in this region.

The frequencies of the traveling eddies can be correlated using two nondimensional groups: the Strouhal number St and the jet-to-wind momentum flux ratio J. Figure 9 shows the result of the correlation. The Strouhal number decreases rapidly with the jet-to-wind momentum flux ratio in region A. The decreasing rate in transition region B decelerates. The Strouhal number approaches an almost constant value of about 0.35 as the jet-to-wind momentum flux ratio increases to the region C, the jet momentum dominant region. The Strouhal number and the jet-to-wind momentum flux ratio can be correlated logarithmically by

$$St = \exp(-0.3894\ \ell_n J - 0.6247) \tag{1}$$

The trajectories of the traveling organized structures can be depicted by the bisector of the long time exposure shadowgraph images of the path that the eddies pass over. Following the nondimensional parameters $\bar{X}$ and $\bar{Z}$ used by Pratte and Baines[24] for correlation of the wind-blown jet in the range of $25 \le J \le 1225$, the trajectories of the traveling eddies in this study for $J < 20$ can be correlated by

$$\bar{Z} = 0.86\bar{X}^{0.37} \qquad \text{for the near field} \tag{2}$$

and

$$\bar{Z} = 1.07\bar{X}^{0.21} \qquad \text{for the far field} \tag{3}$$

Figure 10 shows the results of the correlation. The momentum flux ratio, which implicitly appears in the nondimensional parameters, plays an important role in the jet behavior. Also shown in Fig. 10 for comparison are the lines representing the near nozzle solution obtained theoretically by Brzustowski[19] for flames in the burner-detached regime and the experimental correlation obtained by Pratte and Baines[24] for the visible centerline of an air jet emanating at high jet-to-wind momentum flux ratios from a hole on a wall and seeded with an aerosol spray. Because the stability domain of the burner-detached flames covers the regimes of lower crossflow velocities and much higher jet velocities than that of the flames in the burner-attached regime, and because of the nonlinear behavior of the jet/wind interaction, the loci of the trajectories in these two categories reside on different levels.

Coherent Structure and Flame Behavior

The transition region, region B as shown in Fig. 3, covers the regime of characteristic flame mode IV. In flame mode IV, the dual flame, the fuel jet, and the crossflow have about the same velocities. The fuel jet momentum is slightly dominant in this flame mode. The fuel jet on the symmetric center plane is not bent as much as that in an off-center area and hence makes the jet body look split, as shown in Fig. 4d. The traveling coherent structure

follows the upper trajectory and the side-skimmed jet fluid follows the lower trajectory. The short time exposure schlieren picture of Fig. 11a shows the indistinguishable orientation of the coherent structure in this mode. The long time exposure schlieren photograph in Fig. 11b records the split images of the jet body. The split streams correspond to the formation of the dual flame, which is shown in Fig. 12. The flame length reaches a minimum as the flame appears most obviously dual. Because the jet-to-wind momentum flux ratios (about 1) in this regime are not high enough to generate the streamwise counter-rotating vortices,[16] no evidence showing the influence of these structures on the dual-flame mode was found.

In the regime of the flickering flame mode, the flame flickers between bright and dark appearances periodically. Figure 13 shows the flow patterns and flame appearances in bright and dark modes of the flickering flames. Figures 13a and 13b describe the flow and appearance of the flickering flame in the bright mode. Figures 13c and 13d are for the dark mode. The soot-radiating zone in color photograph Fig. 13b starts earlier and has a longer and fatter radiating orange zone in the downstream area, compared with that in Fig. 13d. The switching between bright and dark appearances is because of the soot yield. The higher the soot yield, the brighter the flame appears. The schlieren photographs in Figs. 13a and 13c show the different flow patterns in bright and dark modes. The primary difference is the trigger point of the unsteady vortices. In the bright mode, as shown in Fig. 13a, the unsteady structures are found to start at about one and a half burner diameters downstream from the tip of the burner. The strong coherent vortices are not formed in the near burner region. While in the dark mode, as shown in Fig. 13d, the vortices start earlier and are more coherent than they are in the bright mode. The strong entrainment and mixing processes proceed as the vortices travel downstream and penetrate into the blue turbulent combustion zone. The combustion with better mixing and diffusion between fuel and air reduces the soot yield and hence makes the flame look darker. The onset point of the coherent structures moves upstream and downstream periodically and the motion remains in phase with the flickering of the flame. Although the formation of vortices leading to the flickering of the flames is shown, the mechanism leading to the unsteady triggering of the vortices in this region is still unclear.

Conclusions

The flame behavior and flow structure in the stability domain of the combusting jet in the crossflow in the burner-attached regime are investigated experimentally. Six typical flame modes are identified. The coherent structures evolving from the upwind side of the bent jet body display various characteristic modes. The reduced frequency of the traveling coherent structure is logarithmically correlated to the jet-to-wind momentum flux ratio. The Strouhal number of the traveling eddies approaches almost a constant value of 0.35 at high jet-to-wind momentum flux ratios. The trajectories of the traveling coherent structure depicted by the bisector of the eddy traveling avenue are correlated by two nondimensional coordinates which are related to the jet-to-wind momentum flux ratio. The split of the jet fluid is found to correspond to the formation of the dual flame. The flickering of the flame is closely related to the unsteady triggering of the organized structure.

Acknowledgments

This study was supported by the National Science Council of the Republic of China under Grant NSC 82-0401-E-011-193. The authors appreciate the help of David Han, M. Z. Lin G. M. Bear, and C. L. Lin for their assistance in the construction of the wind tunnel.

References

[1]Brown, G. L., and Roshko, A, "On Density Effects and Large Structure in Turbulent Mixing Layers," *Journal of Fluid Mechanics,* Vol. 64, July 1974, pp. 775–816.

[2]Yule, A. J., "Large-scale Structure in the Mixing Layer of a Round Jet," *Journal of Fluid Mechanics,* Vol. 89, Dec. 1978, pp. 413–432.

[3]Coles, D., "The Uses of Coherent Structure," AIAA Paper 85-0506, Jan. 1985.

[4]Broadwell, J. E., and Briedenthal, R. E., "A Simple Model of Mixing and Chemical Reaction in a Turbulent Shear Layer," *Journal of Fluid Mechanics,* Vol. 125, Dec. 1982, pp. 397–410.

[5]Mungal, M. G., Dimotakis, P. E., and Broadwell, J. E., "Turbulent Mixing and Combustion in a Reacting Shear Layer," *AIAA Journal,* Vol. 22, No. 6, 1984, pp. 797–800.

[6]Mungal, M. G., and Dimotakis, P. E., "Mixing and Combustion with Low Heat Release in a Turbulent Shear Layer," *Journal of Fluid Mechanics,* Vol. 148, Nov. 1984, pp. 349–382.

[7]Takeno, T., and Kotani, Y., "Transition and Structure of Turbulent Jet Diffusion Flames," AIAA Paper 77-97, Jan. 1977.

[8]Takagi, T., Shin, H. D., and Ishio, A., "Properties of Turbulence in Turbulent Diffusion Flames," *Combustion and Flame,* Vol. 40, Feb. 1981, pp. 121–140.

[9]Yule, A. J., Chigier, N. A., Ralph, S., Boulderstone, R., and Ventura, J., "Combustion-Transition Interaction in a Jet Flame," *AIAA Journal,* Vol. 19, No. 6, 1981, pp. 752–760.

[10]Takahashi, F., Mizomoto, M., and Ikai, S., "Transition from Laminar to Turbulent Free Jet Diffusion Flames," *Combustion and Flame,* Vol. 48, Oct. 1982, pp. 85–95.

[11]Peters, N., and Williams, F. A., "Liftoff Characteristics of Turbulent Jet Diffusion Flames," AIAA Paper 82-011, Jan. 1982.

[12]Eickhoff, H., Lenze, B., and Leuckel, W., "Experimental Investigation on the Stabilization Mechanism of Jet Diffusion Flames," *Twentieth Symposium (International) on Combustion,* The Combustion Institute, Pittsburgh, PA, 1984, pp. 311–318.

[13]Gollahalli, S. R., Savas, Ö, Huang, R. F., and Rodriquez Azara, J. L., "Structure of Attached and Lifted Gas Jet Flames in Hysteresis Region," *Twenty-first Symposium (International) on Combustion,* The Combustion Institute, Pittsburgh, PA, 1986, pp. 1463-1471.

[14]Savas, Ö., and Gollahalli, S. R., "Flow Structure in Near-Nozzle Region of Gas Jet Flames," *AIAA Journal,* Vol. 24, No. 7, 1986, pp. 1137–1140.

[15]Kalghatgi, G. T., "Blow-Out Stability of Gaseous Jet Diffusion Flames Part II: Effect of Cross Wind," *Combustion Science and Technology,* Vol. 26, Nos. 5 and 6, 1981, pp. 241–244.

[16]Gollahalli, S. R., Brzustowski, T. A., and Sullivan, H. F., "Characteristics of a Turbulent Propane Diffusion Flame in a Cross-Wind," *Transaction of CSME,* Vol. 3, No. 4, 1975, pp. 205–214.

[17]Botros, P. E., and Brzustowski, T. A., "An Experimental and Theoretical Study of the Turbulent Diffusion Flame in Cross Flow," *Seventeenth Symposium (International) on Combustion,* The Combustion Institute, Pittsburgh, PA, 1978, pp. 389–397.

[18]Kalghatgi, G. T., "The Visible Shape and Size of a Turbulent Hydrocarbon Jet Diffusion Flame in a Cross-wind," *Combustion and Flame,* Vol. 52, No. 1, 1983, pp. 91–106.

[19]Brzustowski, T. A., "The Hydrocarbon Turbulent Diffusion Flame in Subsonic Cross Flow," AIAA Paper 72-222, Jan. 1977.

[20]Birch, A. D., Brown, D. R., Fairweather, M., and Hargrave, G. K., "An Experimental Study of a Natural Gas Jet in a Cross-Flow," *Combustion Science and Technology,* Vol. 66, Nos. 4–6, 1989, pp. 217–232.

[21]Askari, A., Bullman, S. J., Fairweather, M., and Swaffield, F., "The Concentration Field of a Turbulent Jet in a Cross-Wind," *Combustion Science and Technology,* Vol. 73, Nos. 1–3, 1990, pp. 463–478.

[22]Ellzey, J. L., Berbee, J. G., Tay, Z. F., and Foster, D. E., "Total Soot Yield from a Propane Diffusion Flame in Cross-Flow," *Combustion Science and Technology,* Vol. 71, Nos. 1–3, 1990, pp. 41–52.

[23]Huang, R. F., Savas, Ö., and Gollahalli, S. R., "Flow Field in the Near Burner Region of a Partially Lifted Turbulent Gas Jet Flame in Cross Flow," *1992 Heat and Mass Transfer in Fire and Combustion Systems,* ASME HDT 223, 1992, pp. 105–110.

[24]Pratte, B. D., and Baines, W. D., "Profiles of the Round Turbulent Jet in a Cross Flow," *Journal of the Hydraulics Division,* ASCE, Vol. 92, No. HY6, 1967, pp. 53–64.